

Supplementary Materials and Methods

Data with separate floating vegetation classes

In attempts to classify more species-specific classes in the reference data that more closely aligned with our field observations (see first section of Methods), we created datasets by classifying points as either floating ‘EFB + Lily spp.’ or floating ‘Duckweed spp.’ given that these species were generally discernible in the UAS imagery (Fig. 1b). Distinguishing Submergent or Emergent points into individual species was not possible at either spatial resolution. The final sample size was $N = 316$ in the 11 cm dataset (Duckweed spp. = 103, EFB + Lily spp. = 64, Emergent = 83, Submergent = 66). The final sample size of the aggregated points was $N = 249$ in 11 cm dataset (Emergent = 83, Floating = 100, Submergent = 66) and $N = 229$ in the 3 cm dataset (Emergent = 83, Floating = 94, Submergent = 53). After combining the Floating class, we removed a random portion of the points to achieve a more balanced sample size between classes.

Using field data to interpret RF outputs

Mohammadi et al. (*in prep*) collected random-stratified quadrat plot points on community vegetation data (including EFB abundance) and various covariates throughout vegetation zones at Alpena during July-August 2019. Using the spectral signals from imagery captured with our UAS during July 2019, Mohammadi et al. (*in prep*) utilized an unsupervised classification algorithm in ArcGIS 10.7 to define the boundaries of each vegetation zone throughout the flight footprint. The outputs from this approach resulted in five unique vegetation zones in the study site: Floating vegetation, Mixed (floating and submergent) vegetation, Open Water, Submergent vegetation, and Emergent Typha (*Typha × glauca*). Then, the authors collected plant community and environmental data at ten randomly distributed points throughout each zone in the flight footprint ($N = 50$). We then used these points as an additional dataset to interpret the outputs from our RF classification algorithm.

Supplementary Results

Classification with separate floating vegetation classes

Upon processing of the field data, we assigned all training points to one of the four following classes: floating ‘Efb + Lily spp.’, floating ‘Duckweed spp.’, ‘Submergent Vegetation,’ and ‘Emergent Vegetation.’ We hypothesized that this configuration of classes in the training data would yield spectrally distinct values in the UAS bands and would be structurally separable. However, preliminary results indicate that model results on the disaggregated data were less accurate than when we combined the two floating classes (‘Efb + Lily spp.’ and ‘Duckweed spp.’ into one single Floating class (Table A1 vs. Table 5 in manuscript), likely due to their similar spectral and structural values (Fig. A1). Therefore, we decided to maintain the combination of vegetation samples and run models on three vegetation classes (‘Emergent’, ‘Floating’, Submergent’) for the remainder of analyses.

Table S1. Confusion matrix for the 11 cm ‘Multispectral + DSM + Rugosity’ model on the disaggregated vegetation classes recorded in the field: floating Efb + Lily spp., floating Duckweed spp., Submergent, and Emergent vegetation. Reference data are actual recorded classes from the field as well as reference points determined from the imagery and predicted classes at test points were generated from the random forest model. The greyed out diagonal values are the number of points correctly classified by the model, with the bold value in the bottom right cell representing the overall accuracy of the model (sum of the diagonal values/the total number of points * 100). Producer’s and User’s Accuracy (PA & UA) are displayed in % accuracy.

		Reference					
		Efb + Lily spp.	Duckweed spp.	Submergent	Emergent	Total	UA
Predicted	Efb + Lily spp.	1871	395	334	347	2947	63.49
	Duckweed spp.	923	4096	666	59	5744	71.31
	Submergent	41	359	2025	56	2481	81.62
	Emergent	365	300	275	3638	4578	79.47
	Total	3200	5150	3300	4100	15,750	
	PA	58.47	79.53	61.36	88.73		73.4

Spectral and structural profiles

For the dataset with separate floating classes, we observed the greatest spectral separability in the NDVI band, with Emergent and ‘EFB + Lily spp.’ points exhibiting higher values than either ‘*S. polyrhiza*’ or Submergent vegetation points (Fig. A1). The Emergent class also yielded higher structural and textural values than either of the three other classes (Fig. A1).

After combining the floating classes, we observed the greatest separability in % mean reflectance, in both pixels and image objects, in the NDVI, Red Edge, and NIR bands from both flight dates and for all three vegetation classes (Figs. A2-A5). Pixels and image objects also exhibited similar spectral and structural profiles across both spatial resolutions and flight dates, with greater standard error around for image object means in some bands (Figs. A4-A5).

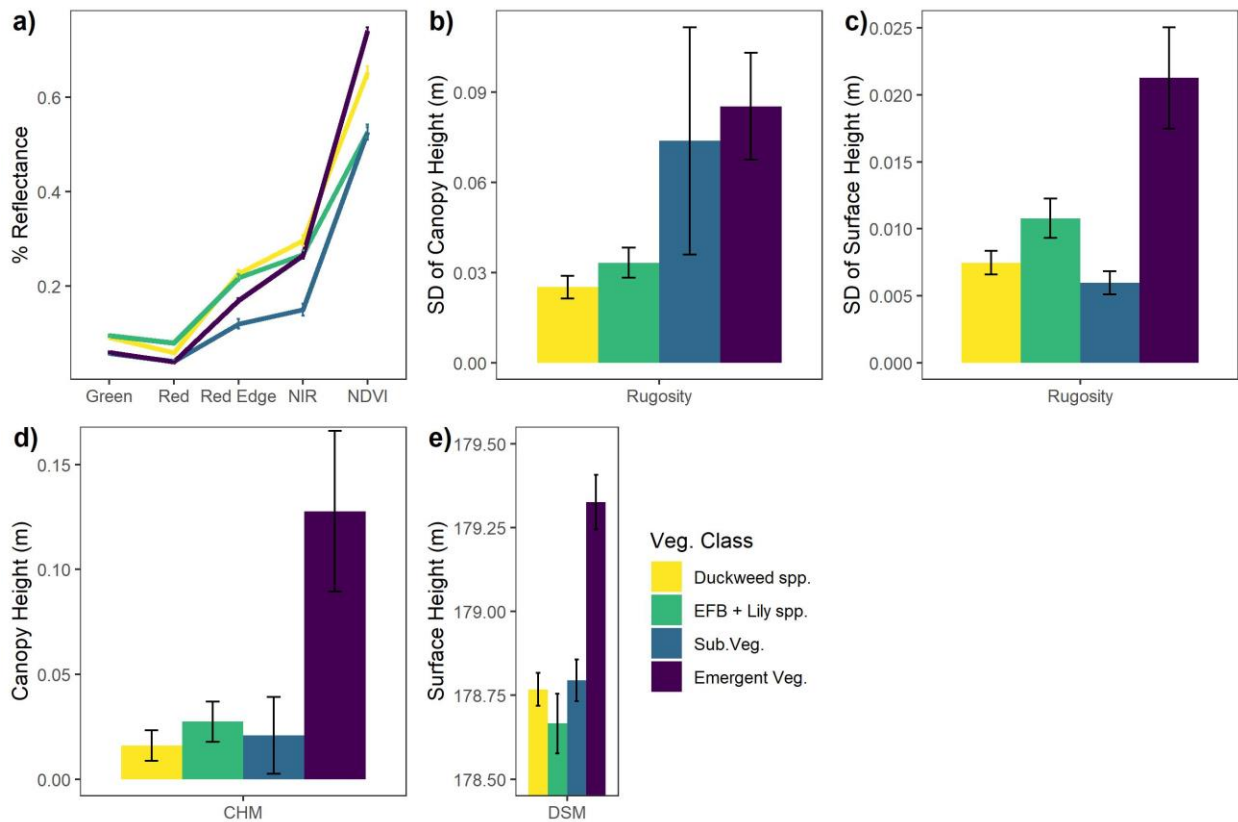


Figure S1. Spectral (a), structural (d,e), and textural (b,c) profiles of the disaggregated vegetation classes: Emergent, Submergent, floating EFB + Lily spp., and floating Duckweed spp. (*S. polyrhiza*) extracted from mean pixel values in the 11cm dataset. All bands, except Rugosity and Surface Height (m), are % reflectance values calibrated for each band during pix4D processing.

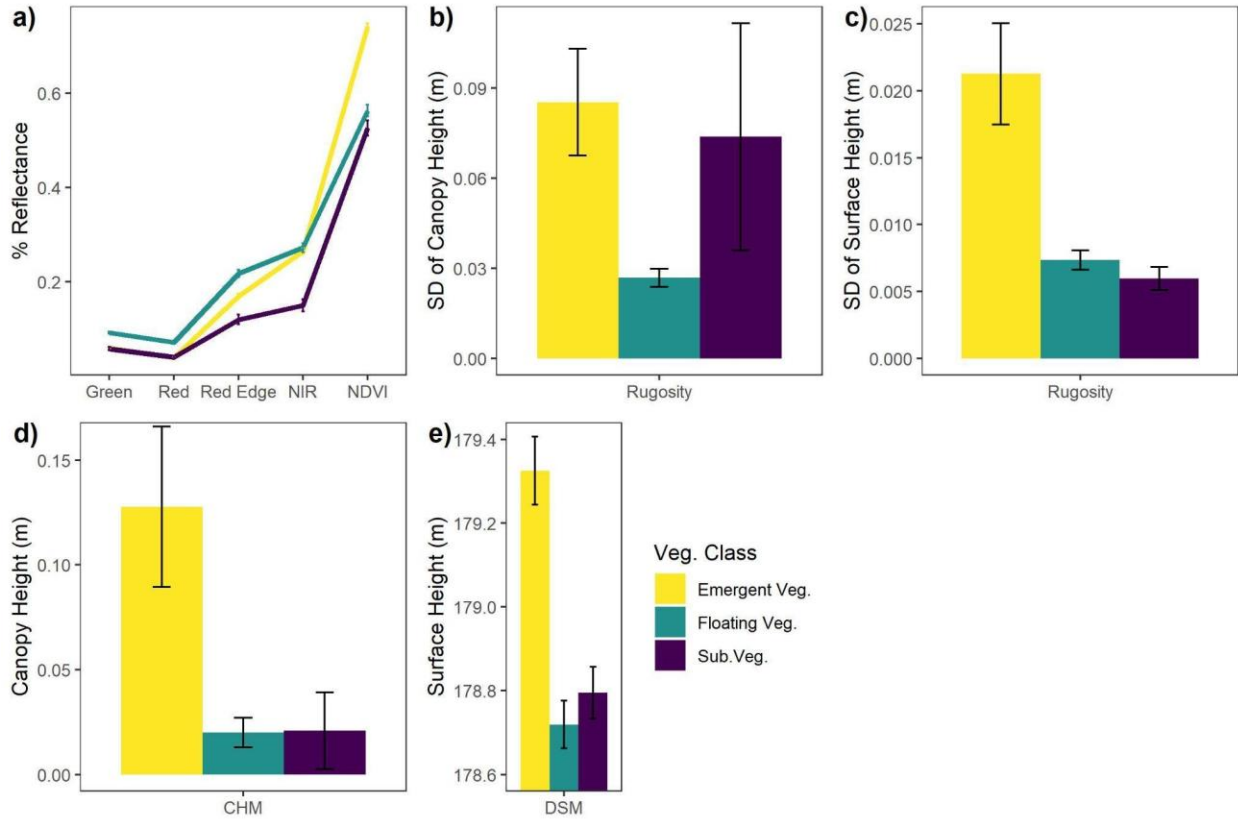


Figure S2. Spectral (a), textural (b,c), and structural (d,e) profiles of the three aggregated vegetation classes: Emergent, Submergent, Floating Vegetation, extracted from mean pixel values 11cm dataset. All bands, except Rugosity and Surface Height (m), are % reflectance values calibrated for each band during pix4D processing.

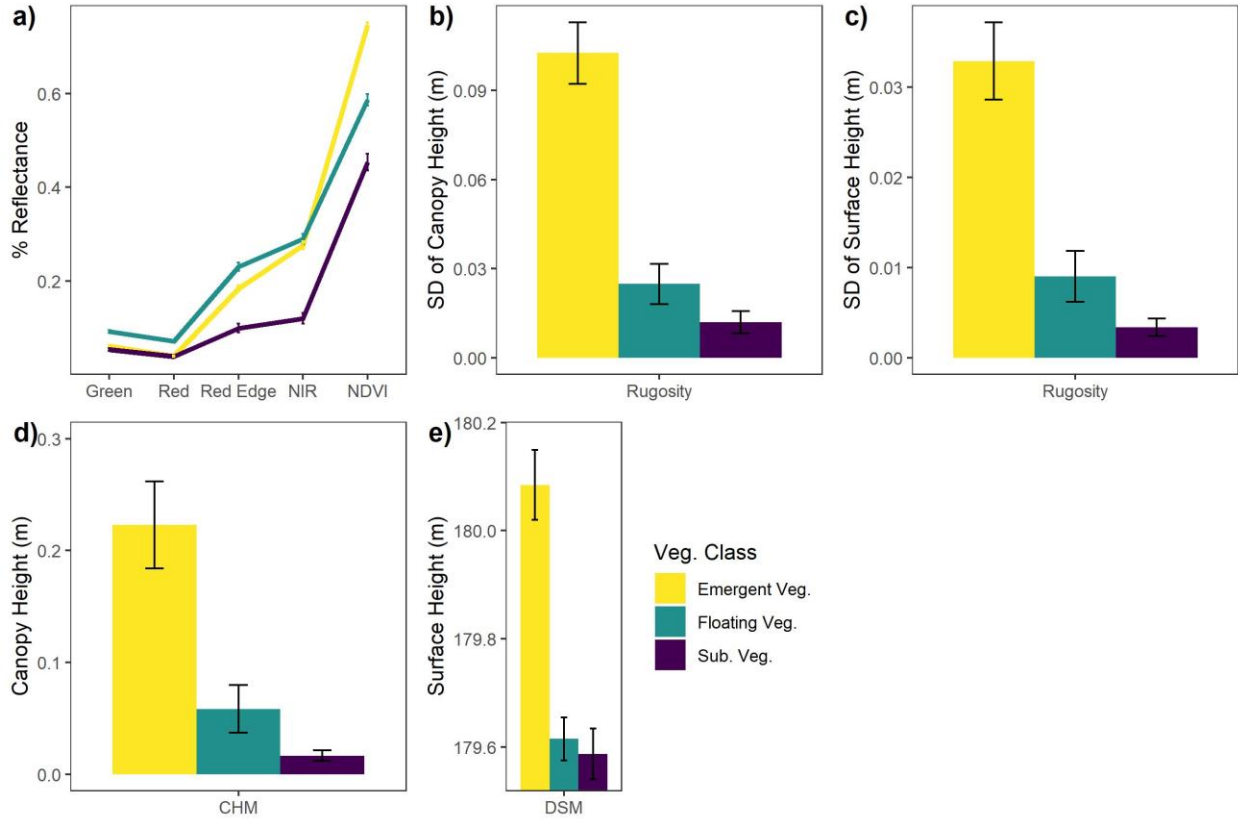


Figure S3. Spectral and textural profiles of the three vegetation classes: Emergent, Submergent, Floating Vegetation, extracted from mean pixel values in the 3 cm dataset. All bands, except Rugosity and Surface Height (m), are % reflectance values calibrated for each band during pix4D processing.

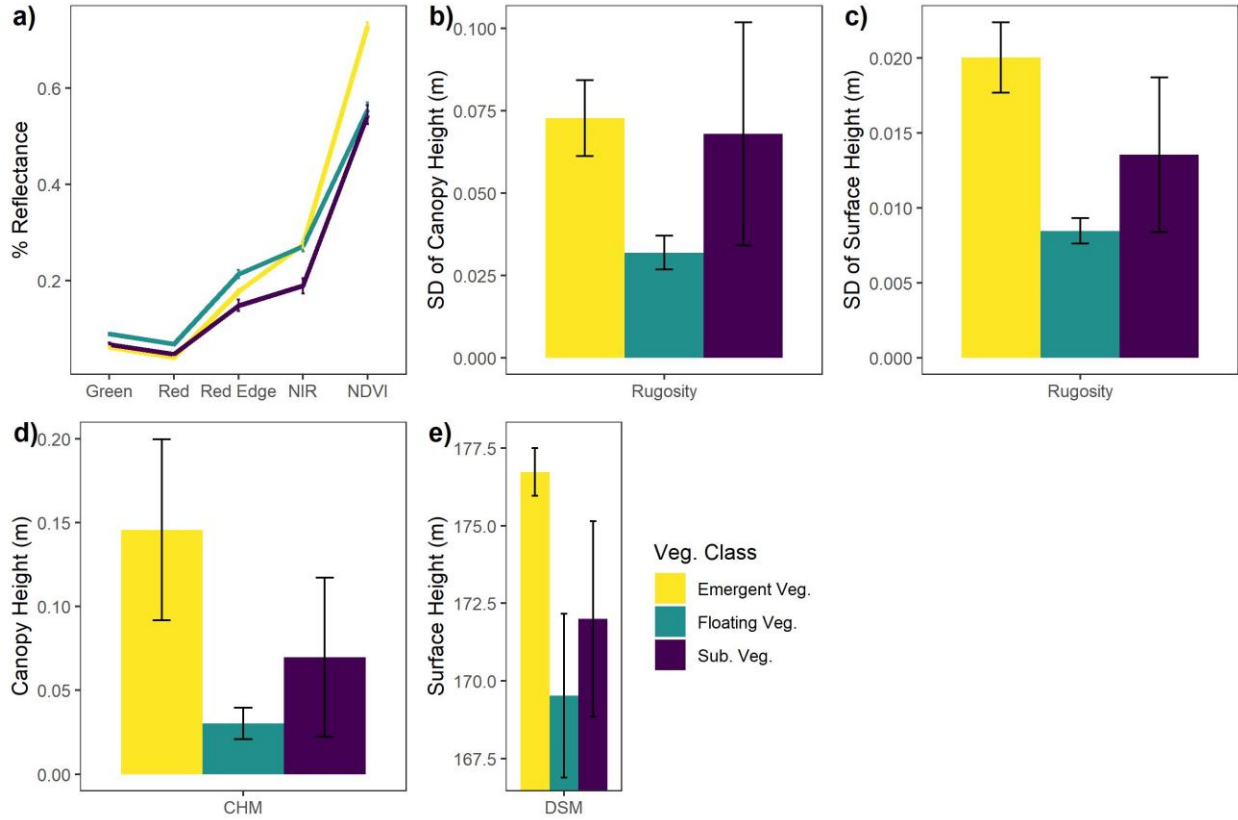


Figure S4. Spectral and textural profiles of the three aggregated vegetation classes: Emergent, Submergent, Floating Vegetation, extracted from mean object values in the 11cm dataset. All bands, except Rugosity and Surface/Canopy Height (m), are % reflectance values calibrated for each band during pix4D processing.

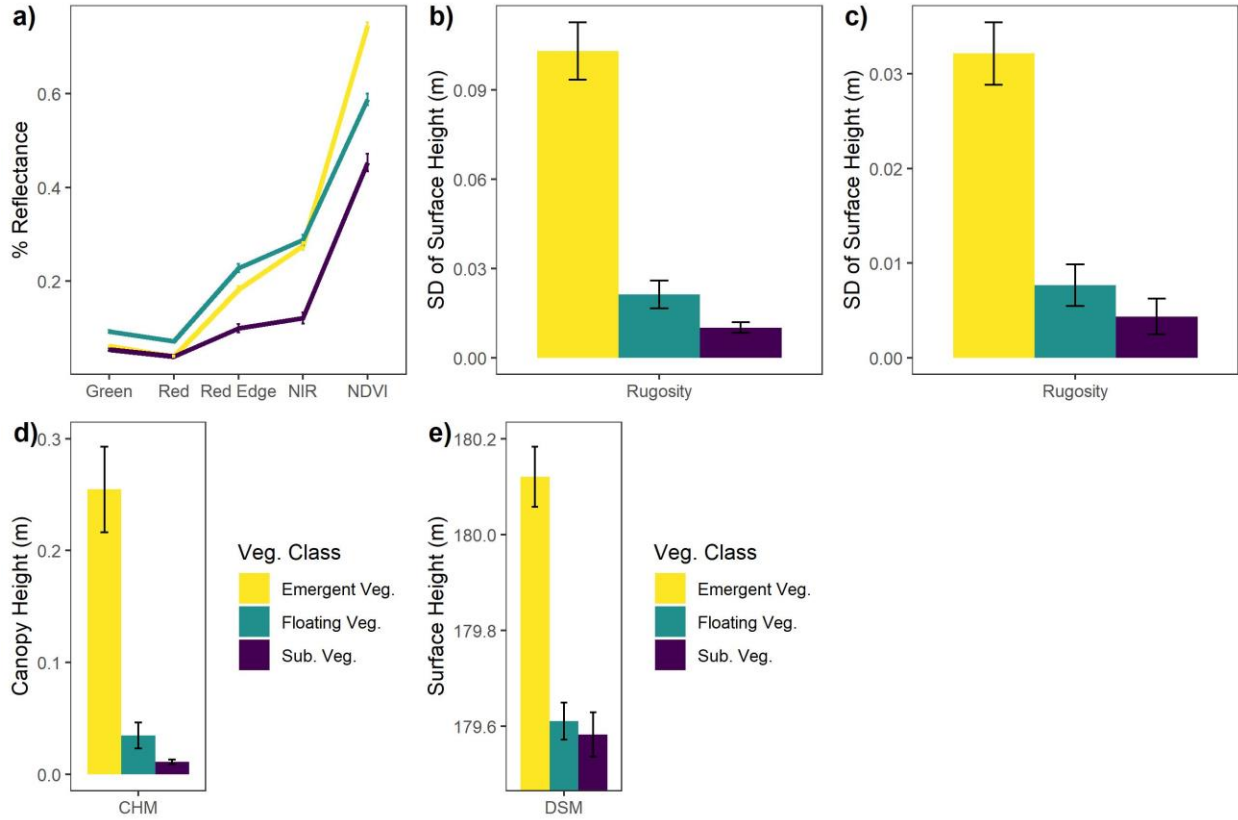


Figure S5. Spectral and textural profiles of the three vegetation classes: Emergent, Submergent, Floating Vegetation, extracted from mean object values in the 3 cm dataset. All bands, except Rugosity and Surface Height (m), are % reflectance values calibrated for each band during pix4D processing.

Object summaries from optimal segmentation algorithms

Overall, the 3 cm imagery with its optimal segmentation parameters produced smaller mean object areas for each vegetation class than the 11 cm imagery, indicating that the 3 cm imagery included more spectral and structural detail at a finer spatial scale (Table A2).

Table S2. Mean object size (\pm SD, in m^2) of the points for the four vegetation classes from the reference data overlaid on the optimal segmentation outputs for the OBIA.

Vegetation Class	Mean Object Area (\pmSD, in m^2) from DSM Data	Mean Object Area (\pmSD in m^2) from CHM Data
<i>11 cm spatial resolution</i>		
EFB + Lily Spp.	1.67 (\pm 2.2)	23.03 (\pm 10.5)
Duckweed Spp.	2.94 (\pm 3.1)	36.27 (\pm 137.6)
Submergent Veg.	823.19 (\pm 1147)*	720.85 (\pm 635)*
Emergent Veg.	8.57 (\pm 14.1)	32.01 (\pm 25.2)
<i>3 cm spatial resolution</i>		
EFB + Lily Spp.	1.71 (\pm 10.1)	2.71 (\pm 8.3)
Duckweed Spp.	2.75 (\pm 15.8)	12.54 (\pm 64)
Submergent Veg.	0.85 (\pm 3.3)	6.24 (\pm 15)
Emergent Veg.	0.12 (\pm 0.16)	1.11 (\pm 0.8)

* The large mean values are driven by a few very large image objects (in area) produced by the segmentation algorithm for the Submergent class in the 11 cm imagery.

Band importance

The most important bands for predicting the three vegetation classes differed between the high and very-high resolution datasets (Figs. A6-A17). For the very-resolution data, the NDVI and/or Rugosity bands were the most important (% increase in mean squared error when those bands are not included in models) for both the pixel- and object-based approaches (Figs. A6-11). For the high-resolution data, the Red, Green, and/or NDVI bands were the most important (Figs. A12-A17).

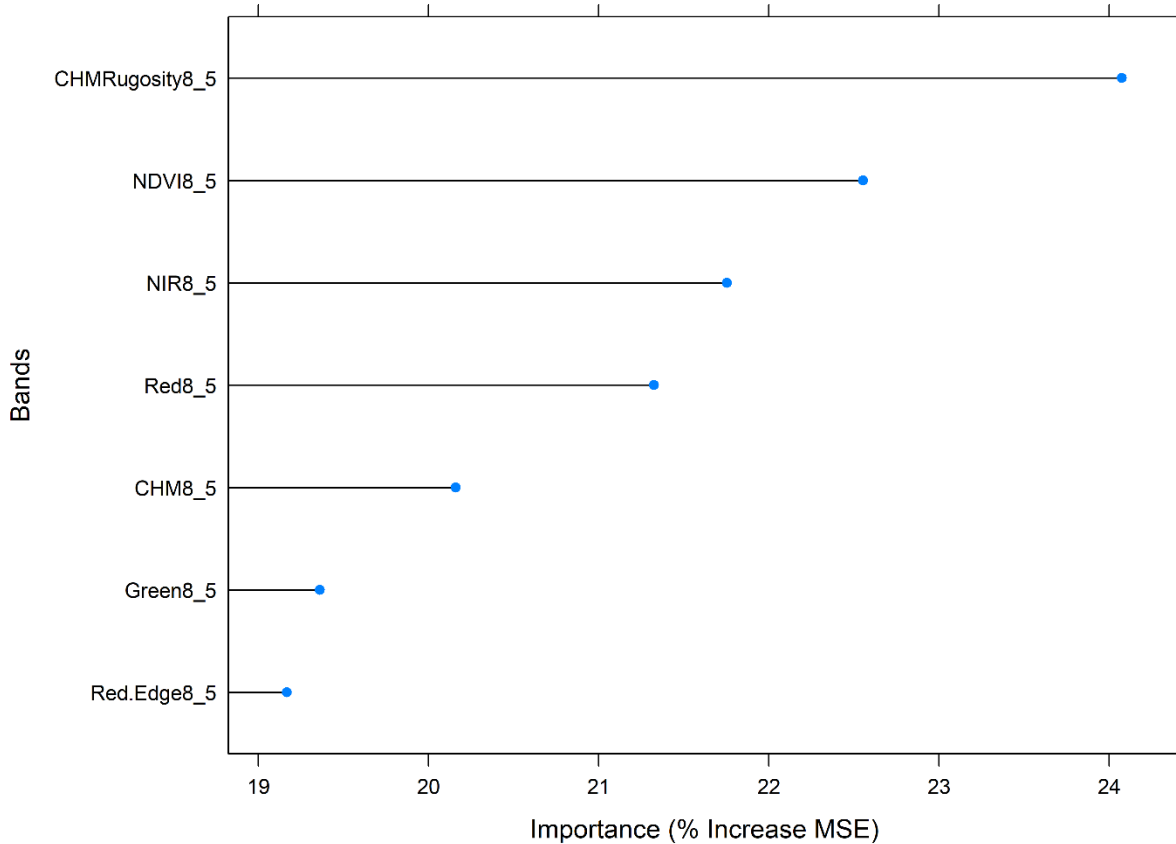


Figure S6. Mean Decrease in Gini Importance (Importance on x-axis) for each mean and SD reflectance/structure for the 7 bands in the pixel-based “Multispectral + CHM” model of the 3 cm data (resampled to 15 cm). Importance is based on % increase in mean squared error (MSE) for each band on the out of bag data for each tree in the RF and then computed after permuting a variable (band).

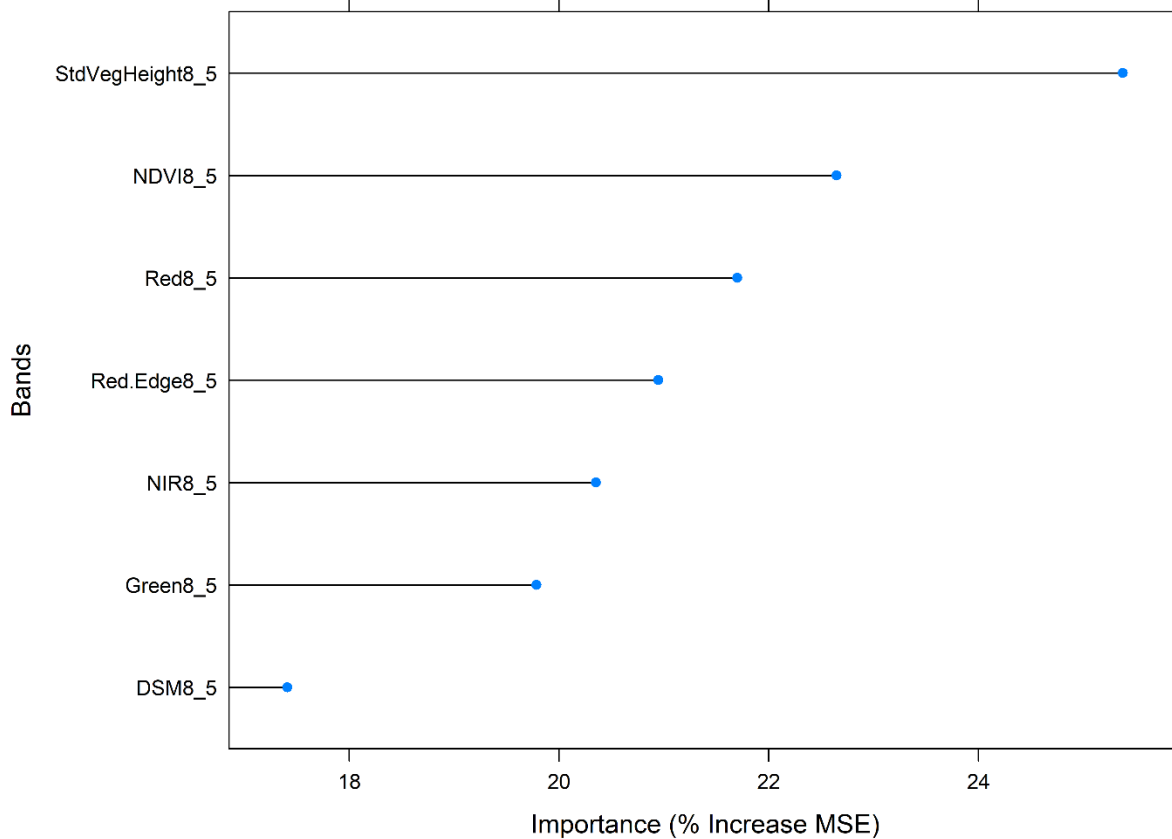


Figure S7. Mean Decrease in Gini Importance (Importance on x-axis) for each mean and SD reflectance/structure for the 7 bands in the pixel-based “Multispectral + DSM” model of the 3 cm data. Importance is based on % increase in mean squared error (MSE) for each band on the out of bag data for each tree in the RF and then computed after permuting a variable (band).

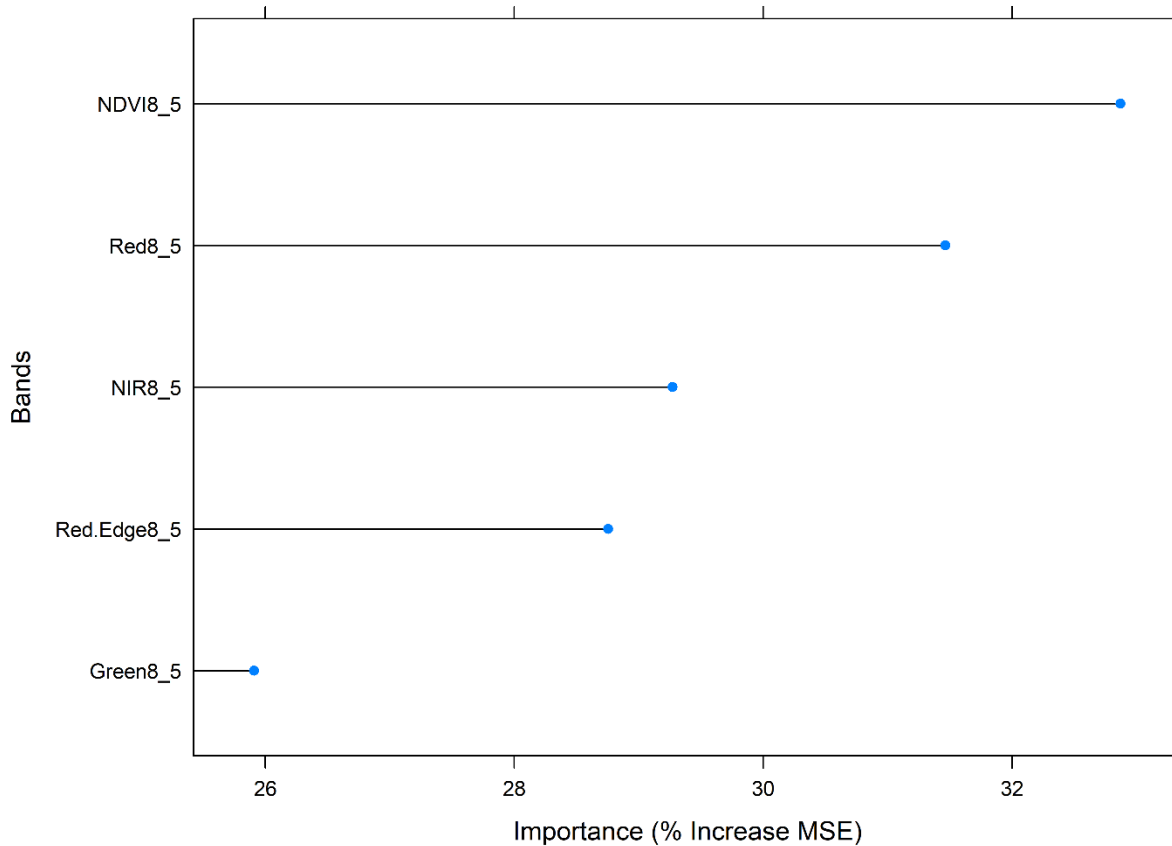


Figure S8. Mean Decrease in Gini Importance (Importance on x-axis) for each mean and SD reflectance/structure for the five bands in the pixel-based “Multispectral Only” model of the 3 cm data. Importance is based on % increase in mean squared error (MSE) for each band on the out of bag data for each tree in the RF and then computed after permuting a variable (band).

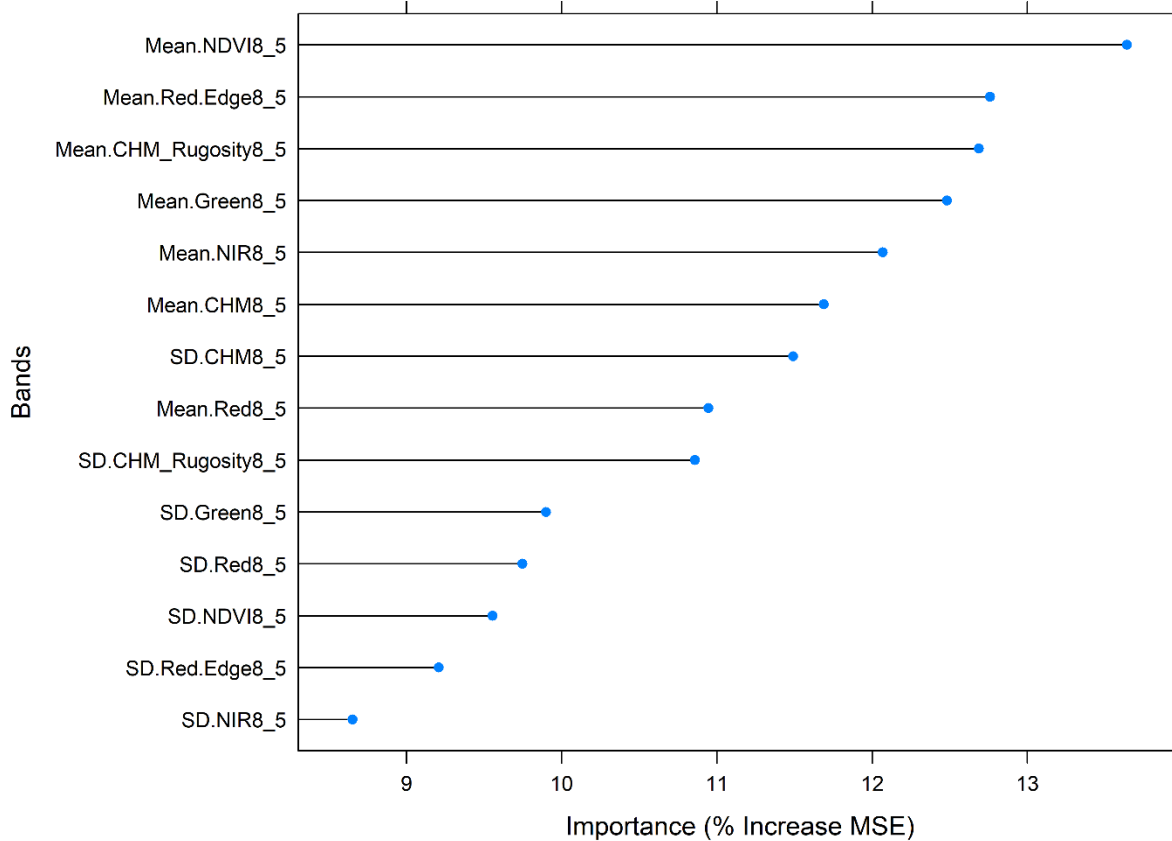


Figure S9. Variable importance for each mean and SD reflectance/structure of the segments (image-objects) for the 14 bands in the object-based ‘Multispectral + Both CHM’ model of the 3 cm data (resampled to 15 cm). Importance is based on % increase in mean squared error for each band on the out of bag data for each tree in the RF and then computed after permuting a variable (band).

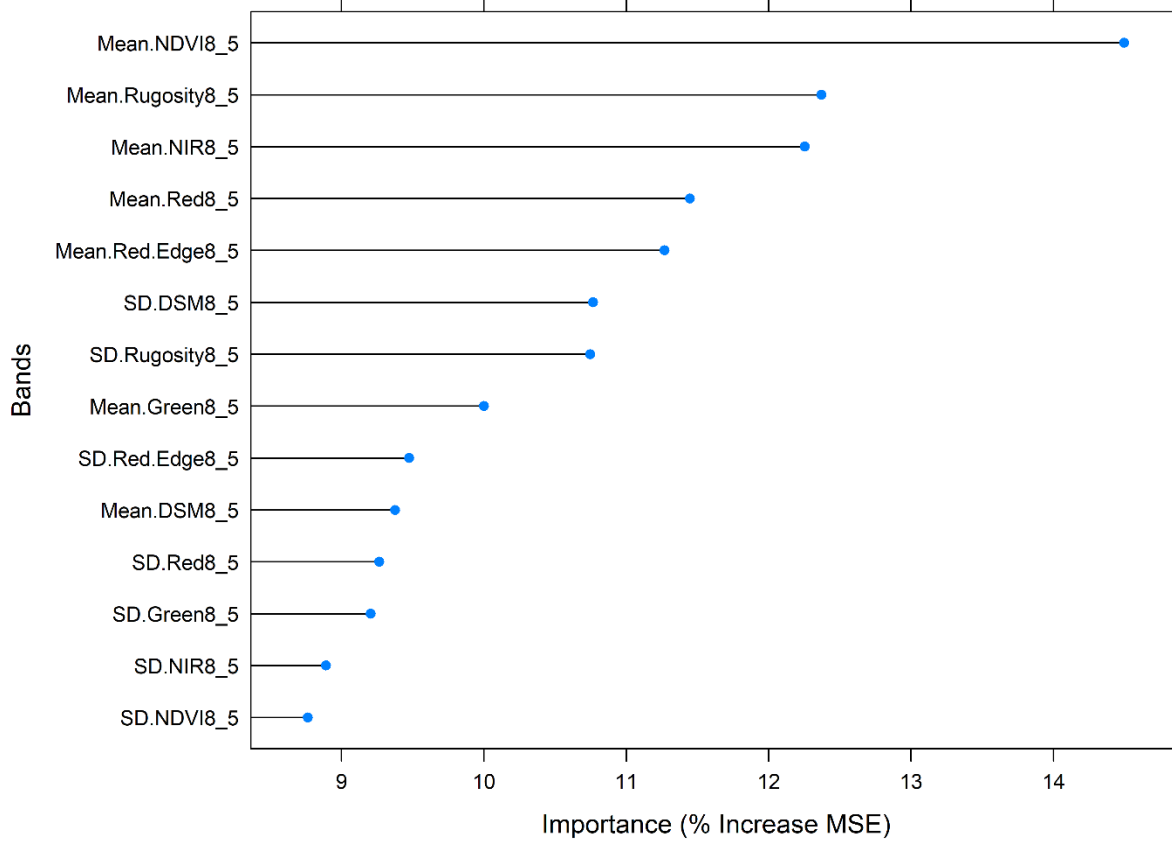


Figure S10. Variable importance for each mean and SD reflectance/structure of the segments (image-objects) for the 14 bands in the object-based ‘Multispectral + Both DSM’ model of the 3 cm data. Importance is based on % increase in mean squared error for each band on the out of bag data for each tree in the RF and then computed after permuting a variable (band).

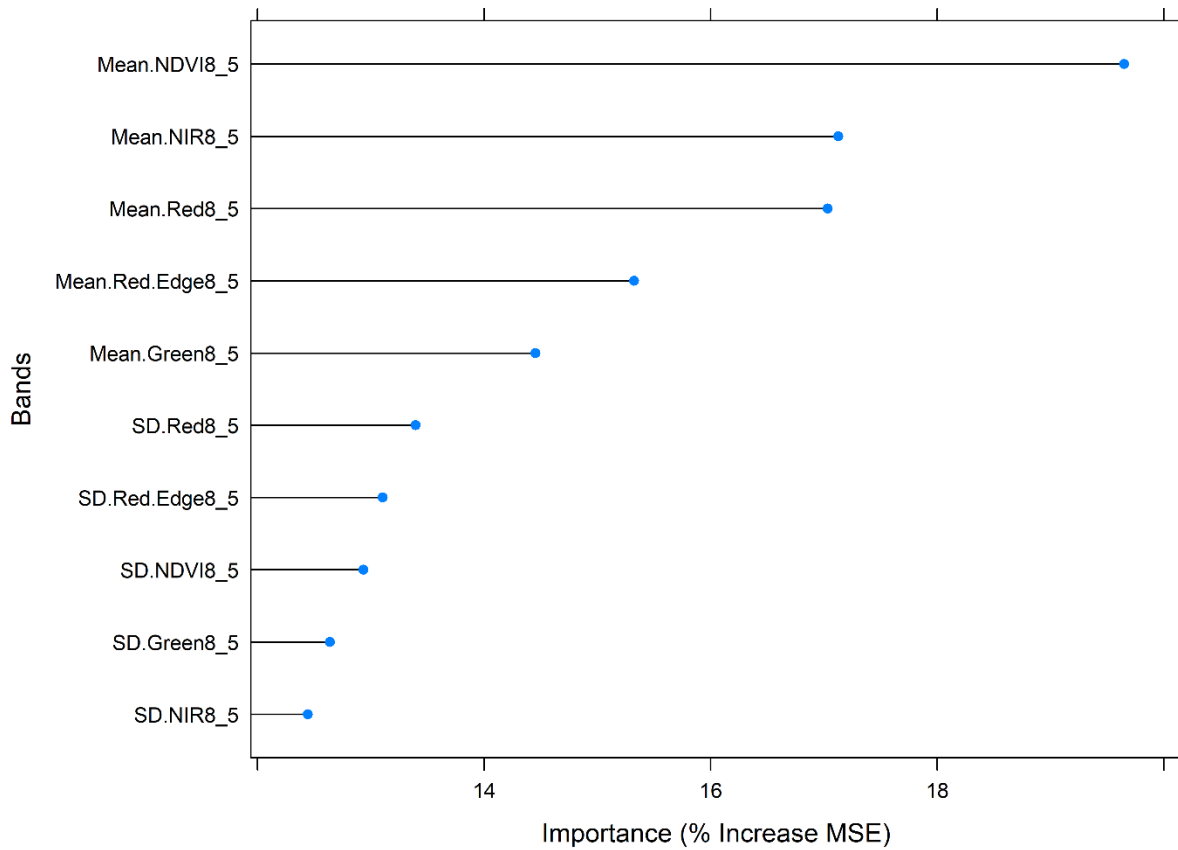


Figure S11. Variable importance for each mean and SD reflectance/structure of the segments (image-objects) for the 10 bands in the object-based ‘Multispectral + Only’ model of the 3 cm data. Importance is based on % increase in mean squared error for each band on the out of bag data for each tree in the RF and then computed after permuting a variable (band).

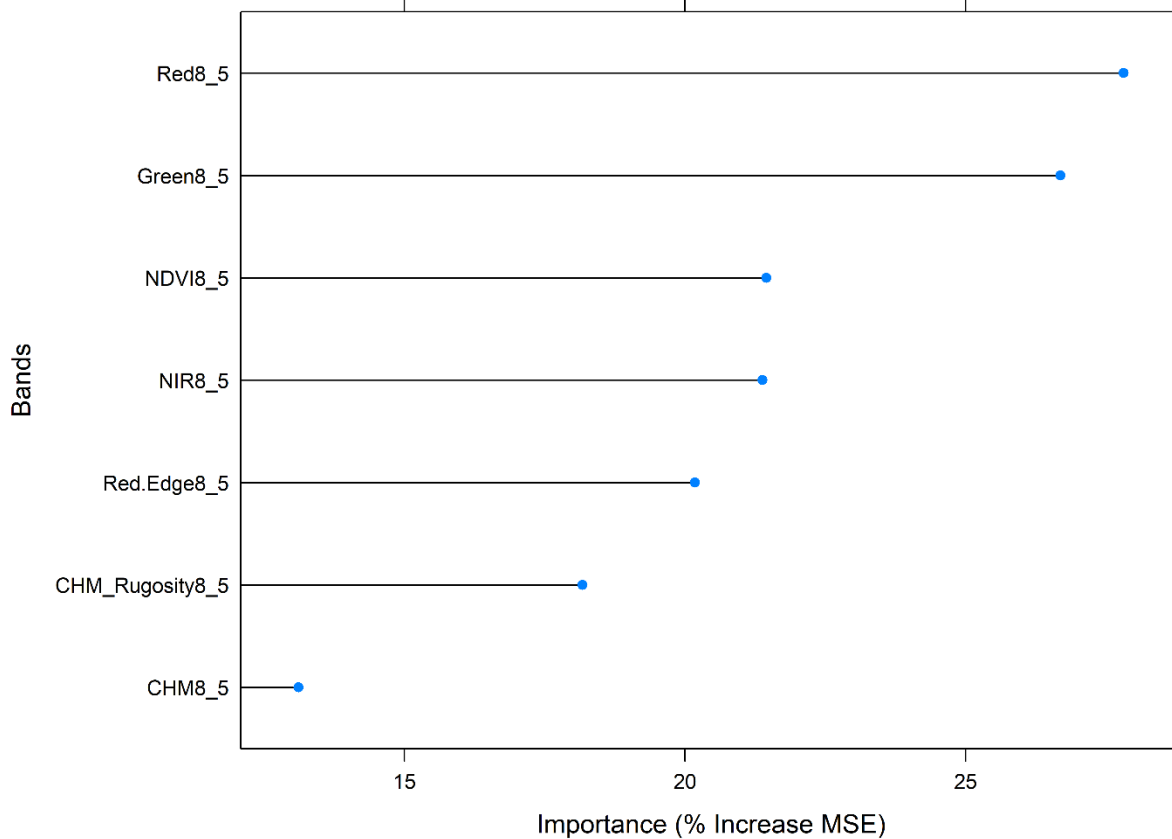


Figure S12. Mean Decrease in Gini Importance (Importance on x-axis) for each mean and SD reflectance/structure for the 7 bands in the pixel-based “Multispectral + CHM” model of the 11 cm data (resampled to 55 cm). Importance is based on % increase in mean squared error (MSE) for each band on the out of bag data for each tree in the RF and then computed after permuting a variable (band).

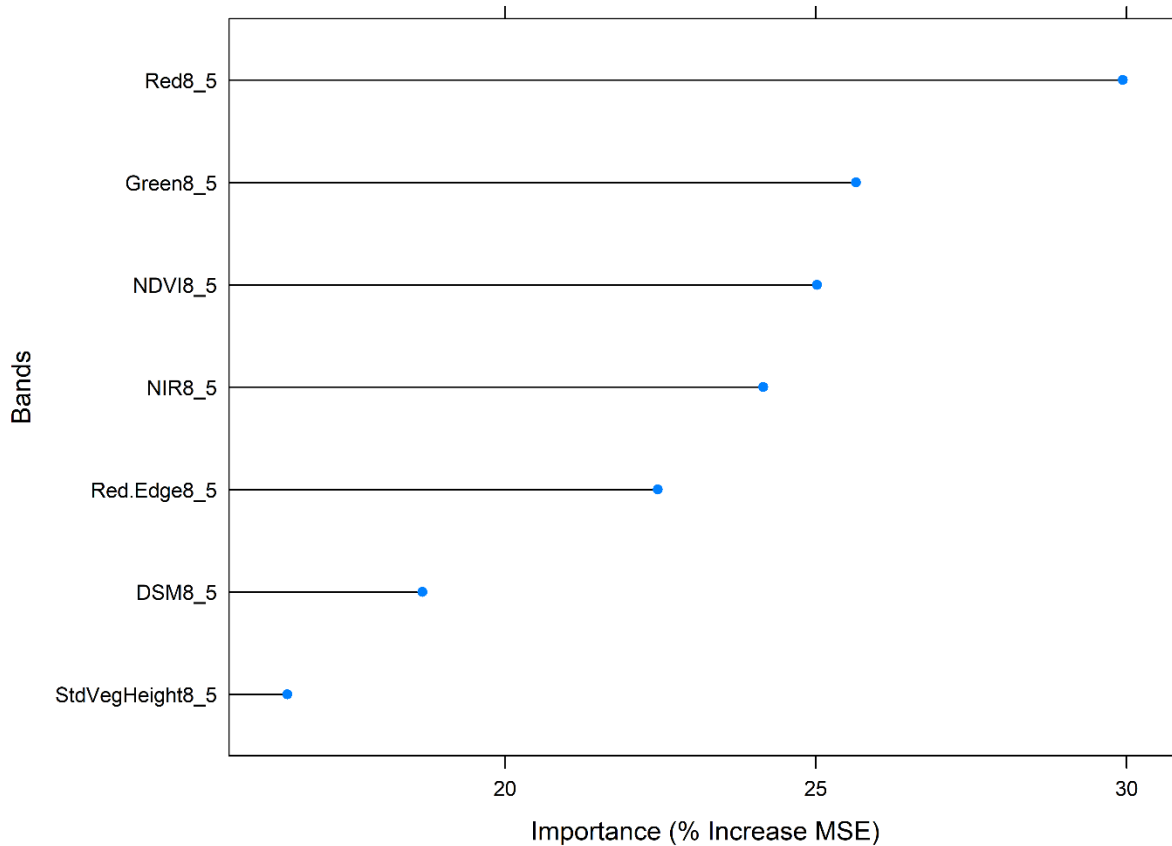


Figure S13. Mean Decrease in Gini Importance (Importance on x-axis) for each mean and SD reflectance/structure for the 7 bands in the pixel-based “Multispectral + DSM” model of the 11 cm data. Importance is based on % increase in mean squared error (MSE) for each band on the out of bag data for each tree in the RF and then computed after permuting a variable (band).

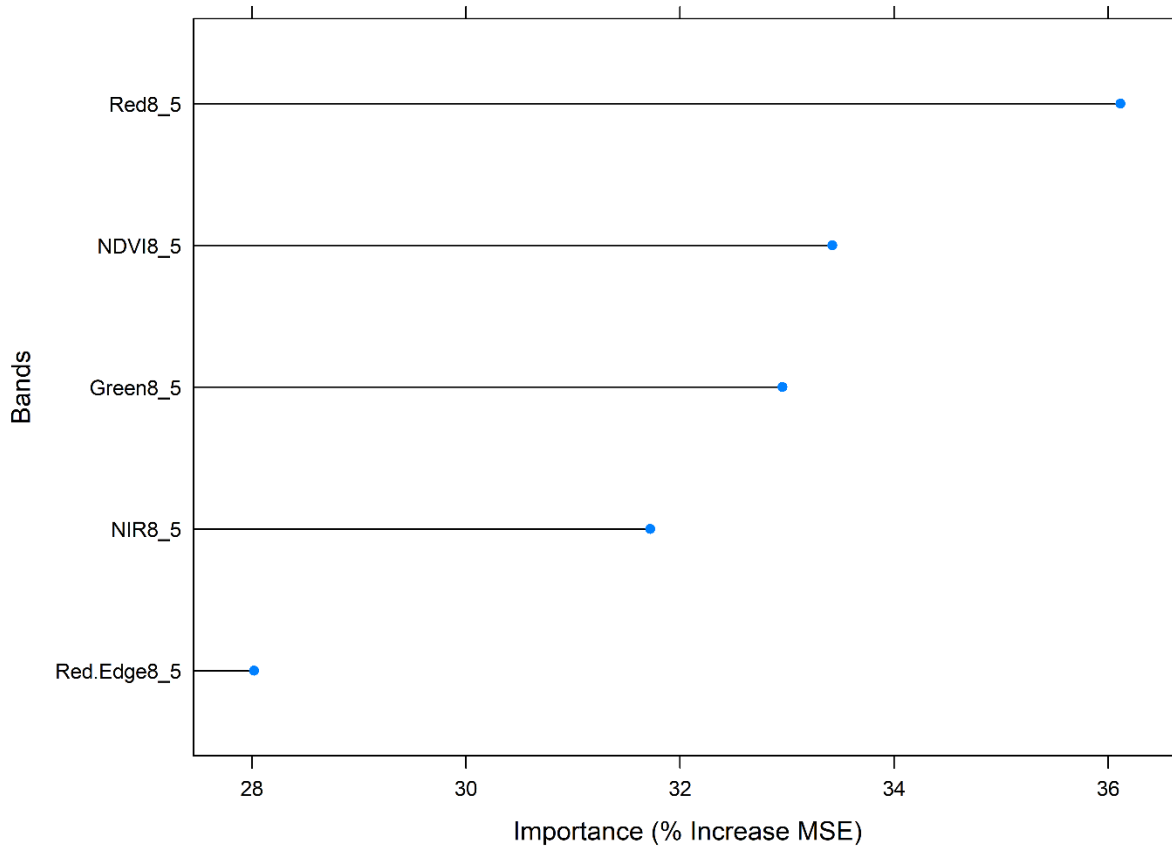


Figure S14. Mean Decrease in Gini Importance (Importance on x axis) for each mean and SD reflectance/structure for the 7 bands in the pixel-based “Multispectral Only” model of the 11 cm data. Importance is based on % increase in mean squared error (MSE) for each band on the out of bag data for each tree in the RF and then computed after permuting a variable (band).

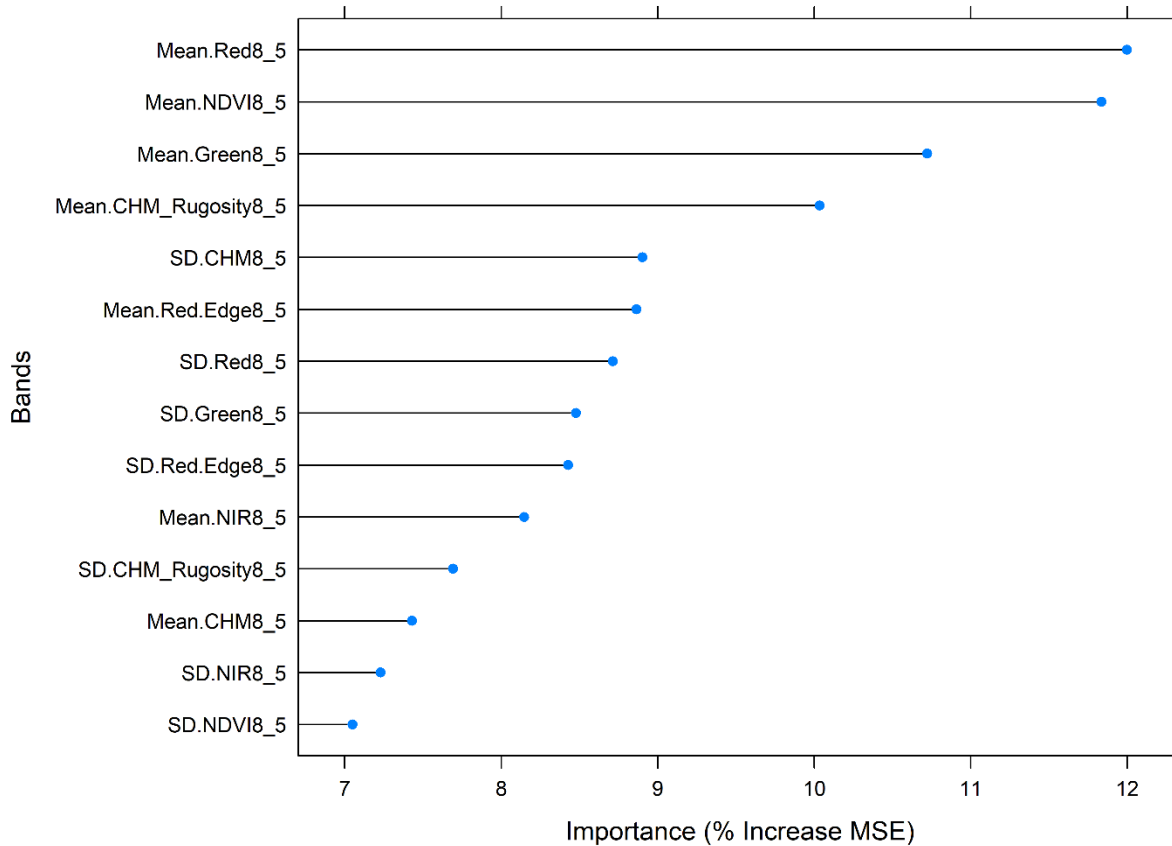


Figure S15. Mean Decrease in Gini Importance (Importance on x axis) for each mean and SD reflectance/structure of the segments (image-objects) for the 14 bands in object-based “Multispectral + CHM” model of the 11 cm data (resampled to 55 cm). Importance is based on % increase in mean squared error (MSE) for each band on the out of bag data for each tree in the RF and then computed after permuting a variable (band).

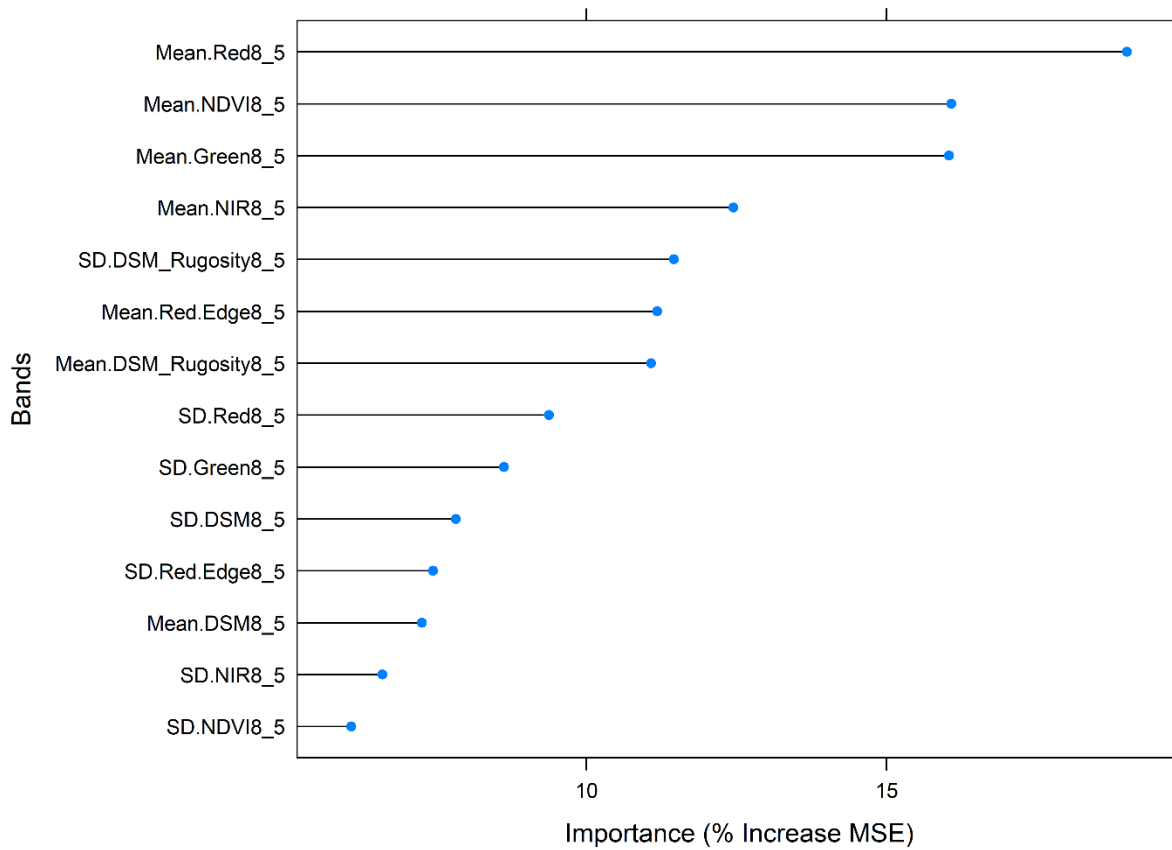


Figure S16. Mean Decrease in Gini Importance (Importance on x axis) for each of the 14 bands in the object-based ‘Multispectral + DSM’ model of the 11 cm data. Importance is based on % increase in mean squared error (MSE) for each band on the out of bag data for each tree in the RF and then computed after permuting a variable (band).

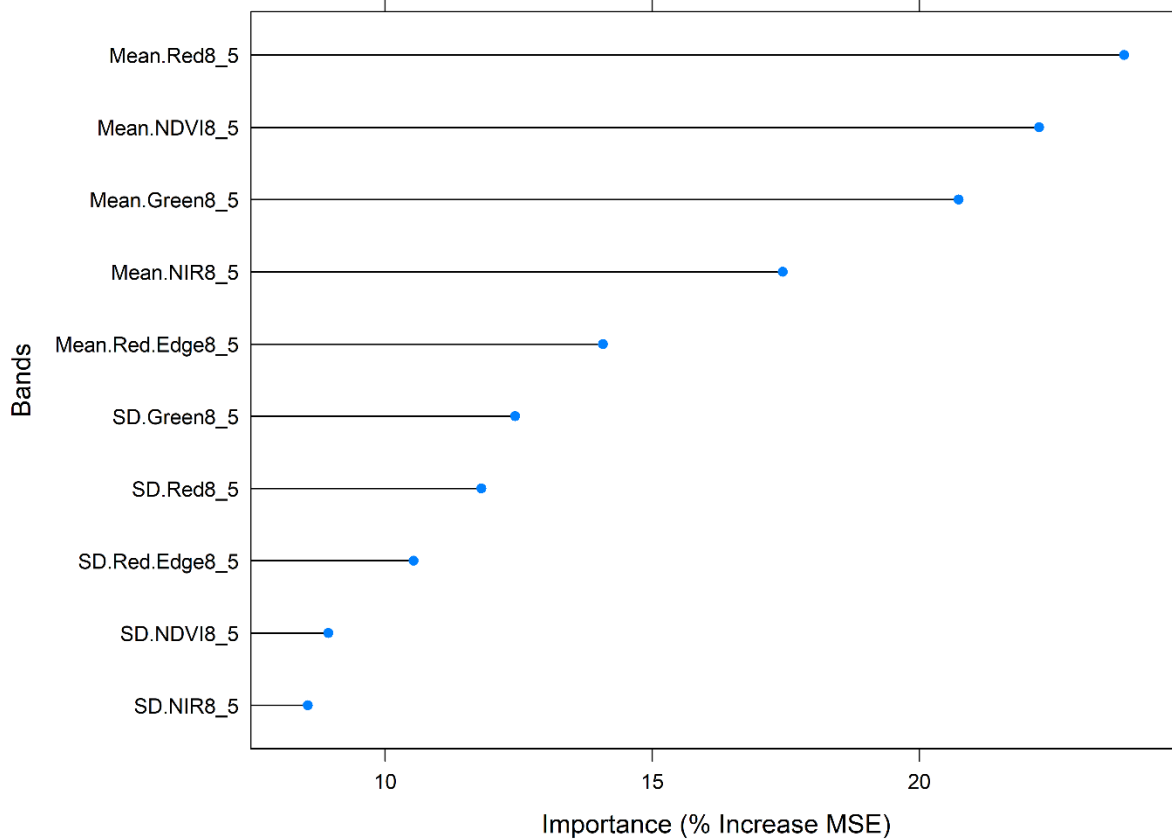


Figure S17. Mean Decrease in Gini Importance (Importance on x axis) for each of the 10 bands in the “Multispectral Only” dataset object-based approach for the 11 cm data. Importance is based on % increase in mean squared error (MSE) for each band on the out of bag data for each tree in the RF and then computed after permuting a variable (band).

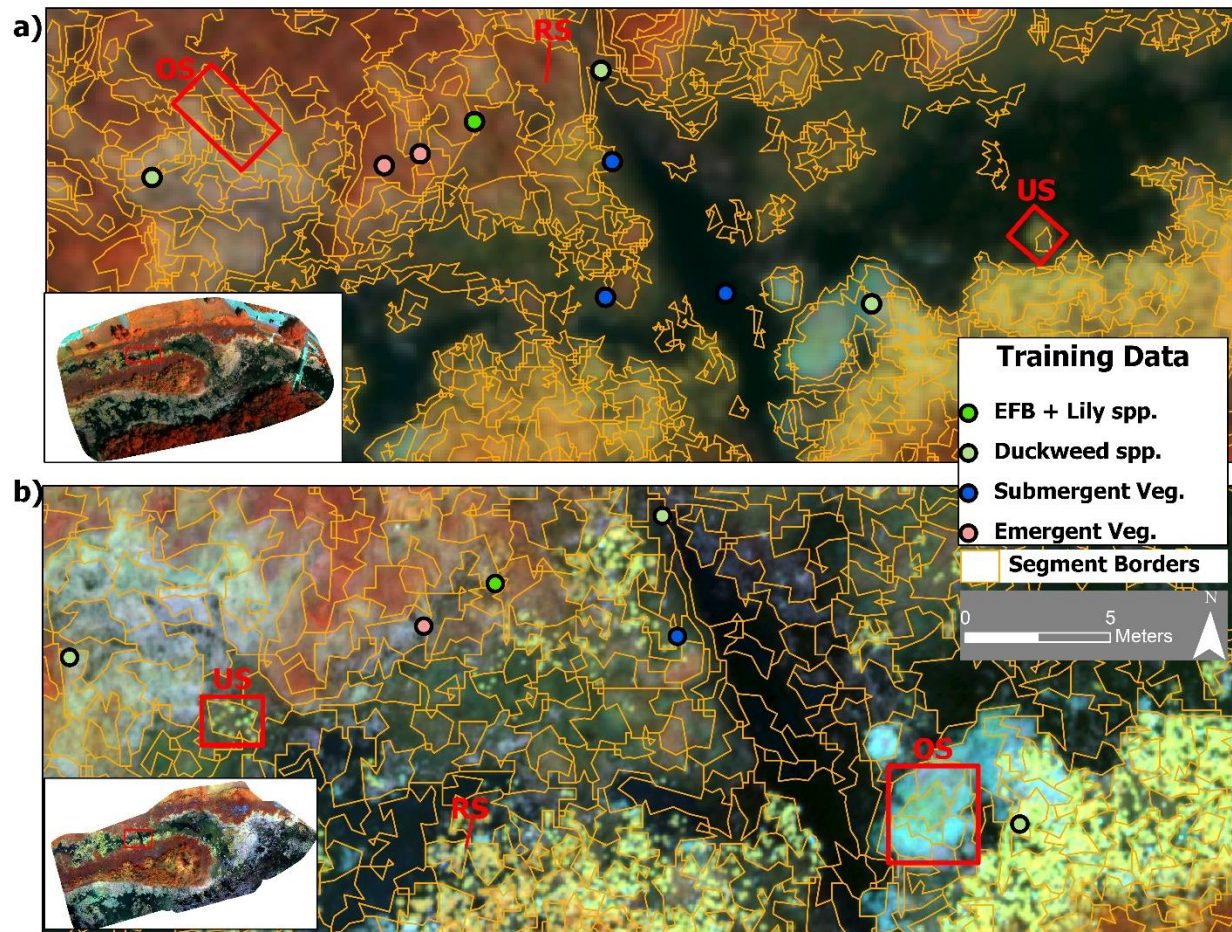


Figure S18 (a) The optimal segmentation layer for the 11 cm dataset (false color composite) with overlaid training data points from the four vegetation classes. **18 (b)** The optimal segmentation layer for the 3 cm imagery of the same area and training data points. Red boxes represent areas with varying degrees of segmentation, where OS indicates “Over-Segmented,” RS indicates “Realistically-Segmented,” and US indicates “Under-segmented.”

Supplementary Discussion

We found that keeping floating ‘EFB + Lily spp.’ and floating ‘Duckweed spp.’ as separate vegetation classes resulted in suboptimal accuracies compared to those when we aggregated all floating species together (Table 3 vs. 4-5). We attribute this finding to the difficulty of assigning points to these classes during the reference data collection, given that the dominant duckweed species (greater duckweed, *Spirodela polyrhiza*) were detected in almost all vegetation zones and classified functional types (Table 6). Although we were seemingly able to distinguish ‘EFB + Lily spp.’ from the more yellow ‘Duckweed spp.’ in both the multispectral and true color imagery (Figs. 1-2), the prevalence of *S. polyrhiza* throughout all floating vegetation likely resulted in classifier confusion between the two floating classes (Table 3). Moreover, many of the mean spectral and structural values were similar between the two separate floating classes (Fig. A1). Merging these two classes into one ‘Floating’ class generally resulted in greater spectral and structural separability compared to either Submergent or

Emergent vegetation across many of the RS bands (Figs. A2-A5), thereby positively influencing classification accuracies (Wicaksono & Aryaguna 2020). We also note that the delineation of vegetation zones by Mohammadi et al. (*in prep*) was based on UAS imagery from mid-July 2019, potentially contributing to some disagreement between designated vegetation zone and RF-predicted vegetation class (Table 6) since the latter was derived from imagery in August. Nevertheless, we suggest for future studies that aim to detect invasive vegetation in UAS data to prioritize collecting as much ground reference data in the field as reasonably possible to avoid such limitations of assigning classes to training points via RS imagery alone.